

Influence of calcination temperature on the morphology and energy storage properties of cobalt oxide nanostructures directly grown over carbon cloth substrates

R. B. Rakhi · Wei Chen · Dongkyu Cha ·
H. N. Alshareef

Received: 10 July 2013 / Accepted: 31 August 2013 / Published online: 23 September 2013
© The Author(s) 2013. This article is published with open access at Springerlink.com

Abstract Nanostructured and mesoporous cobalt oxide (Co_3O_4) nanowire in flower-like arrangements have been directly grown over flexible carbon cloth collectors using solvothermal synthesis for supercapacitor applications. Changes in the morphology and porosity of the nanowire assemblies have been induced by manipulating the calcination temperature (200–300 °C) of the one-dimensional (1-D) structures, resulting in significant impact on their surface area and pseudocapacitive properties. As the calcination temperature increases from 200 to 250 °C, the flower morphology gradually modifies to the point where the electrolyte could access almost all the nanowires over the entire sample volume, resulting in an increase in specific capacitance from 334 to 605 Fg^{-1} , depending on the nanowire electrode morphology. The 300 °C calcination results in the breakdown of the mesoporous morphology and decreases the efficiency of electrolyte diffusion, resulting in a drop in pseudocapacitance after 300 °C. A peak energy density of 44 Wh kg^{-1} has been obtained at a power density of 20 kW kg^{-1} for the 250 °C calcined sample.

Keywords Supercapacitor · Pseudocapacitance · Calcination · Cobalt oxide · Mesoporous · Specific capacitance

Introduction

Significant research interest has been dedicated over the past decade in the development of lightweight and environmentally friendly efficient energy storage devices to meet the various requirements of modern portable consumer electronics and hybrid electric vehicles [1–5]. Supercapacitors, with their higher power densities, fast charge–discharge rates and excellent cycle stabilities than batteries, and higher energy densities than conventional dielectric capacitors, offer a promising approach to satisfy the increasing power demands of energy storage systems in the twenty-first century [6–8]. Depending on the charge storage mechanisms, supercapacitors are broadly classified into two types: (1) electric double-layer capacitors which are based on high surface area carbon nanomaterials with the capacitance arising from the charge separation at the electrode/electrolyte interface and (2) pseudocapacitors based on transition metal oxides (TMOs) or conducting polymers with an additional Faradaic capacitance arising from fast, reversible redox reactions occurring at or near the solid electrode surface [9, 10]. Performance of a supercapacitor strongly depends on the morphology and properties of its electrodes [11]. An ideal electrode material should have large surface area, high conductivity, suitable pore size distribution, long-term cycle stability and electrochemical reproducibility [11]. Carbon materials possess high conductivity and long-term stability; but have lower specific capacitance as compared to pseudocapacitance materials [12–18]. On the other hand, TMOs exhibit higher specific capacitances, but have lower conductivity than the carbon-based systems [19–24]. Conductivity of TMO-based electrodes can be enhanced by the direct growth of TMOs over conducting substrates; this process also eliminates the use of ancillary conducting material and binder in the electrode fabrication process [5, 25–30].

R. B. Rakhi · W. Chen · D. Cha · H. N. Alshareef (✉)
Materials Science and Engineering, King Abdullah University
of Science and Technology (KAUST), Thuwal 23955-6900,
Saudi Arabia
e-mail: husam.alshareef@kaust.edu.sa

Among the different TMOs, cobalt oxide (Co_3O_4) is a promising candidate for pseudocapacitors due to its easy availability, existence of variable oxidation states of metal ions which facilitate redox transitions, good pseudocapacitive behavior with high pseudocapacitance and stable cycling performance and cost-effectiveness as compared to the popular pseudocapacitor material, ruthenium oxide [21, 31–33]. As the electrochemical performance of Co_3O_4 nanostructures largely depends on their morphology and surface area, the development of controlled synthesis techniques of Co_3O_4 nanostructures with high electroactive area is of great importance [34]. There have been a variety of reports on the synthesis of Co_3O_4 nanostructures with different morphologies by different synthetic routes. He et al. reported the size- and shape-controlled synthesis of monodispersed Co_3O_4 nanocrystals by solubility-controlled liquid-phase reaction process. Cao et al. reported the preparation and growth kinetics of highly ordered Co_3O_4 superstructures with tunable morphologies from simple nanoplates to well-organized cabbage-like structures, and then to microspherical composites using a polyol process. Wang et al. reported the synthesis of mesoporous Co_3O_4 nanorods by a simple hydrothermal method [35]. Reports are also available on the direct growth of Co_3O_4 on conducting substrates. Electrodeposition of Co_3O_4 oxide thin films on different substrates are reported by Kandalkar et al. [36] (copper substrates) and Wu et al. [37] (Ni foam substrate). Qing et al. [27] reported the facile synthesis of Co_3O_4 nanoflowers on Ni foam by a simple solvothermal method. Tummala et al. [38] reported the deposition of nanostructured Co_3O_4 on stainless steel current collectors by plasma spray technique.

Among the various possible morphologies of Co_3O_4 , mesoporous one-dimensional (1-D) nanostructures are best suited for supercapacitor applications as they have the advantages of large surface area, improved electrolyte accessibility and reduced mass and charge diffusion distances [31, 34, 39–42]. Very few reports are available on the direct growth of one-dimensional Co_3O_4 nanostructures over different conducting substrates for supercapacitor applications. Gao et al. [43] reported a specific capacitance of 754 F/g at a current density of 5 mA cm^{-2} for Co_3O_4 nanowire arrays directly grown over nickel foam by a simple template-free method. Zhang et al. [33] reported the facile synthesis of freestanding Co_3O_4 nanowire arrays on Ni foam substrate with a remarkable specific capacitance of 1,160 F/g at a current density of 2 A/g. However, it is well known that the use of Ni foam as a current collector can bring about substantial errors to the specific capacitance values of electrode materials [44]. Carbon-coated flexible textiles can be used as an alternative to the Ni foam [45]. Yang et al. [26] reported the direct growth of Co_3O_4 nanowire network (nanonet) on a carbon fiber paper with a

mass loading of 0.4 mg/cm^2 with a large specific capacitance (1,124 F/g) at a high discharge current density of 25.34 A/g. In a recent work, we reported remarkable pseudocapacitance for self-organized microstructures of mesoporous Co_3O_4 nanowires grown over two different types of carbon paper substrates by a solvothermal method [25]. The work was focused on how the surface texture of paper substrate influenced the morphology and pseudocapacitance of Co_3O_4 . We could achieve Co_3O_4 nanowires which are organized into flower-like morphology over planar graphitized carbon paper and brush-like morphology over fibrous non-graphitized carbon paper substrate. The work dealt with samples calcined at 250 °C. But during the course of study we came across some interesting observations which revealed that the calcination temperature played a crucial role in tuning the pseudocapacitance, morphology and pore size of the sample with flower-like morphology [25].

As the carbon substrate is sensitive to high temperature, extreme care needs to be taken in selecting the suitable calcination temperature, which can dramatically enhance the supercapacitor performance of Co_3O_4 without damaging the carbon substrate. To the best of our knowledge, no detailed reports are available on the influence of calcination temperature on the morphology, pore structure and hence pseudocapacitance of 1-D Co_3O_4 nanostructures grown directly over carbon cloth substrate. We could reproduce the flower-like morphology over graphitized carbon cloth substrate using a solvothermal method. In the present study, we report the effect of calcination temperature on the pseudocapacitive properties of self-organized micro flowers of 1-D Co_3O_4 nanostructures directly grown over graphitized carbon cloth.

Experimental

Synthesis of 1-D Co_3O_4 nanostructures over carbon cloth

One-dimensional Co_3O_4 nanostructures were directly grown over graphitized carbon cloth substrate by a simple solvothermal method. 2 g $\text{Co}(\text{NO}_3)_2 \cdot 6\text{H}_2\text{O}$, 1 g hexa decyl trimethyl ammonium bromide (CTAB) and 6 ml water were dissolved in 30 ml absolute methanol by vigorous magnetic stirring. The resulting solution was then transferred into a 40 ml Teflon-lined stainless steel autoclave. A piece of graphitized carbon cloth (1 cm × 2 cm) was immersed in the growth solution in the autoclave followed by heating the autoclave in an oven at 180 °C for 24 h to allow growth of Co_3O_4 nanoneedles. The substrate covered with products was then washed with H_2O and ethanol, dried in a vacuum at 120 °C for 10 h, and the final product

was denoted as as-prepared sample. The as-prepared samples were then calcined at different temperatures, -200 , 225 , 250 and 300 °C, for 4 h. Calcination temperatures were selected on the basis of thermogravimetric analysis (NETZSCH TG 209 F1 Iris) of as-prepared nanoneedles. The carbon cloth substrate was not able to survive the calcination temperature above 300 °C. The weight of Co_3O_4 deposit was accurately calculated from the difference in the weight of the substrate before the solvothermal process and with Co_3O_4 loading after calcination using an analytical micro balance (XP 26 Mettler Toledo, max 22 g, 0.001 mg of resolution).

General characterization

Co_3O_4 nanostructures were characterized by a powder X-ray diffraction system (XRD, Bruker, D8 ADVANCE) equipped with Cu K_α radiation ($\lambda = 0.15406$ nm). BET surface area of the samples were determined using surface area and porosimetry system 'Micromeritics' (ASAP 2420) at 77 K. Before measurements, the samples were dried at 70 °C for 10 h in a vacuum oven and then degassed at 200 °C for 12 h until the vacuum was <2 $\mu\text{m Hg}$. The surface morphology and microstructure of the samples were investigated by a scanning electron microscopy (SEM, FEI Helios NanoLab) and transition electron microscopy (TEM, FEI Titan).

Electrochemical characterization

Electrochemical measurements were carried out in symmetric two-electrode configurations using a Model 660D electrochemical workstation (CH Instruments). Assembled coin cells for the two-electrode configuration were prepared by sandwiching two identical pieces of Co_3O_4 nanostructures over carbon cloth (each with an area of 0.5×1 cm^2) calcined at a particular temperature by a monolayer polypropylene separator (25 μm thick, Celgard 3501), inside a coin cell (CR2032, MTI), with 30 wt% KOH (Sigma-Aldrich) as electrolyte. The mass of Co_3O_4 in each electrode was approximately 2 mg. The approximate thickness of the active materials on the electrodes was nearly 20 μm . The area of the electrodes was nearly 0.25 cm^2 .

The electrochemical properties of the supercapacitor electrodes were studied by cyclic voltammetry (CV), galvanostatic charge–discharge (CD) and electrochemical impedance spectroscopy (EIS). The CV measurements were conducted in a voltage window between 0 and 0.8 V at a wide range of scan rates, ranging from 1 mV/s to 100 V/s. The CD measurements were also carried out in the same voltage window under a wide range of current densities, from 0.25 to 25 A/g. The EIS was performed in

the frequency range from 100 kHz to 10 mHz at open circuit voltage by applying a 5 mV signal. All measurements were carried out at room temperature.

The specific capacitance (C_{sp}) of symmetric supercapacitors was calculated from the cyclic voltammograms and charge–discharge curves according to Eqs. (1) and (2).

$$C_{\text{sp}} = \frac{2i}{fm} \quad (1)$$

where 'i' is the average cathodic current of the CV loop and 'f' is the scan rate.

$$C_{\text{sp}} = \frac{2}{m} \times \frac{I}{(\Delta V/\Delta t)} \quad (2)$$

where 'I' is the constant current for charge–discharge, $\Delta V/\Delta t$ is the slope of the discharge curve and 'm' is the mass of one electrode. In the present study, for specific capacitance calculation, electrode mass was taken as 2 mg (mass of the Co_3O_4 deposit only).

Results and discussion

1-D Co_3O_4 structures with nanocrystalline and mesoporous nature directly grown over conducting substrates can be considered as ideal candidates for supercapacitor electrodes. Morphology, crystallinity, porosity and capacitive performance of these structures can be varied to a great extent by changing the calcination temperature. Based on the above considerations, in the present work a systematic investigation was conducted to identify the influence of calcination temperature on the morphology and hence the pseudocapacitive properties of 1-D Co_3O_4 nanostructures directly grown over flexible carbon cloth substrate. Self-organization of these nanostructures into flower-like morphologies over flexible carbon cloth collectors was achieved by a simple solvothermal process. Changes in the morphology and porosity of the nanostructure assemblies were induced by manipulating the calcination temperature (200–300 °C) of the one-dimensional (1-D) structures, resulting in significant impact on their surface area and pseudocapacitive properties.

The thermal behaviors of the Co_3O_4 samples were determined by thermogravimetric analysis (TGA) as shown in Fig. 1a. The typical TGA curves of the two precursors clearly display two-step weight loss each, due to dehydration and decomposition of the cobalt carbonate nitrate hydroxide hydrate and $\beta\text{-Co}(\text{OH})_2$ phases. The first weight loss at the lower temperature (<250 °C) is due to the elimination of adsorbed and intercalated water, while the second weight loss from 250 to 300 °C corresponds to the loss of structural water and thermal oxidative

decomposition of the initial products as well as desorption of residual nitrate and carbonate anions. There is no major weight loss at higher temperature in the TGA curve indicating the absence of additional structural changes in those regions. The XRD patterns of the as-prepared and calcined Co_3O_4 samples are shown in Fig. 1b. The as-prepared sample contains a mixture of $\beta\text{-Co}(\text{OH})_2$ (JCPDS 30-0443), cobalt carbonate nitrate hydroxide hydrate (JCPDS50-1891) and Co_3O_4 (JCPDS Card no. 43-1003) as identified from the XRD pattern (Fig. 1i). The sample calcined at 200 °C for 4 h retains (101) peak of the $\beta\text{-Co}(\text{OH})_2$ phase along with the peaks from Co_3O_4 (Fig. 1ii). This residual phase can be removed by increasing the calcination temperature. Samples subjected to calcination temperatures of 225, 250 and 300 °C show identical crystal structures of FCC-type Co_3O_4 nanowires with space group of $\text{Fd}\bar{3}m$ (Fig. 1iii, iv and v). The peaks observed in the XRD pattern can be indexed as (111), (220), (311), (400), (422), (511), (440), (620) and (533) planes of the nanostructured FCC-type Co_3O_4 . Absence of any secondary peaks in the XRD pattern clearly illustrates the complete decomposition of precursors to Co_3O_4 samples after annealing the samples above a temperature of 225 °C.

The nitrogen adsorption and desorption isotherms of the Co_3O_4 samples calcined at different temperatures are shown in Fig. 2a. The Brunauer–Emmett–Teller (BET) surface area values calculated for the as-prepared sample and the samples calcined temperatures of 200, 225, 250 and 300 °C are, respectively, 9.27, 12.89, 13.27, 75.92 and 52.31 m^2/g . All the calcined samples exhibit distinct hysteresis loops in the range of 0.45–1.0 P/P_0 , which suggests the presence of a mesoporous structure. This loop is absent

in the case of the as-prepared sample. The hysteresis loop is prominent in the sample calcined at 250 °C. This can be attributed to the well-formed mesoporous nature with the maximum BET surface area. Xiong et al. [46] reported a BET surface area of 25.12 m^2/g for mesoporous Co_3O_4 nanosheets. Meher and Rao [32] reported the synthesis of mesoporous Co_3O_4 nanowires with a BET surface area of 60 m^2/g . BET surface area value obtained for the Co_3O_4 nanowires in the present study is higher than these reported values, which is favorable for better supercapacitor performance of the composites. Calcination at 300 °C leads to reduction in BET surface area as the smaller particles aggregate to form large crystals in Co_3O_4 structure. Adsorption average pore width (4 V/A by BET) for the as-prepared sample and the samples calcined temperatures of 200, 225, 250 and 300 °C are, respectively, 9.20, 16.39, 17.42, 18.14 and 18.89 nm. The pore size distributions of the samples calculated by desorption isotherms using Barret–Joyner–Halenda (BJH) method are shown in Fig. 2b. BJH Desorption cumulative volume of pores between 1.7000 and 300.0000 nm diameter for the as-prepared sample and the samples calcined temperatures of 200, 225, 250 and 300 °C are 0.04570, 0.05174, 0.06449, 0.10361 and 0.17601 cm^3/g , respectively.

SEM and TEM images of as-prepared samples are shown in Fig. 3. SEM images (Figs. 2a and b) show self-organization of nanoneedles into flower-like morphology on the surface of the graphitized carbon cloth. The nanoneedles have varying lengths of 1–15 μm and diameters <100 nm. From TEM (Fig. 3c) and HRTEM (Fig. 3d) images, it is clear that the nanoneedle exhibits a smooth texture and single crystalline feature.

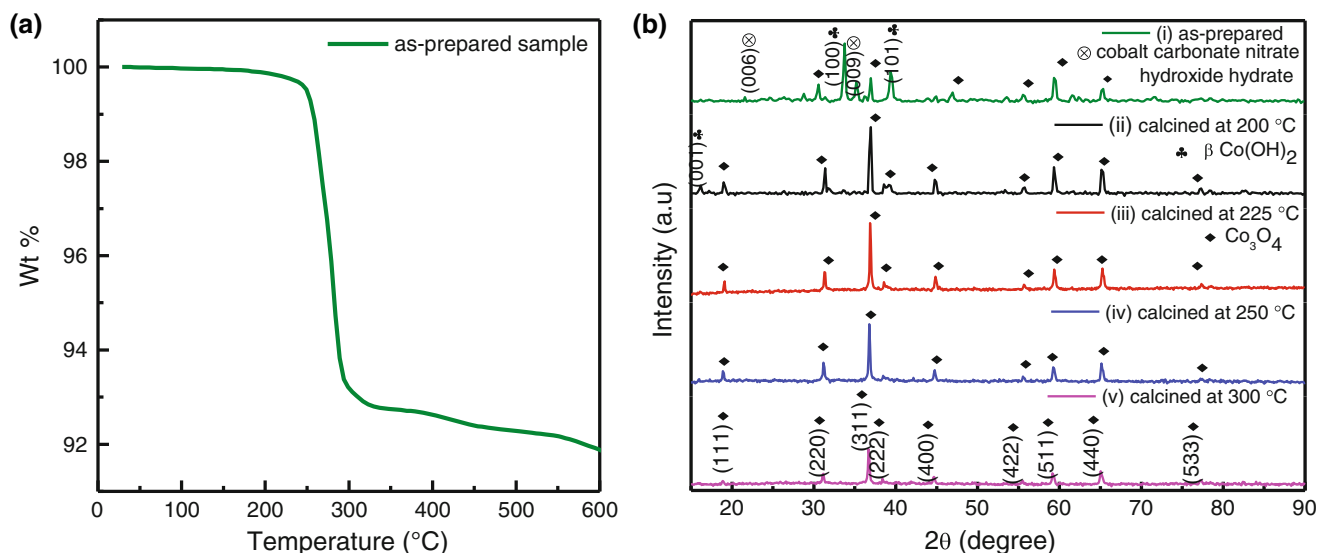


Fig. 1 **a** TGA curve of the as-prepared sample; **b** powder X-ray diffraction pattern of (i) as-prepared sample, (ii) sample calcined at 200 °C, (iii) sample calcined at 225 °C, (iv) sample calcined at 250 °C and (v) sample calcined at 300 °C

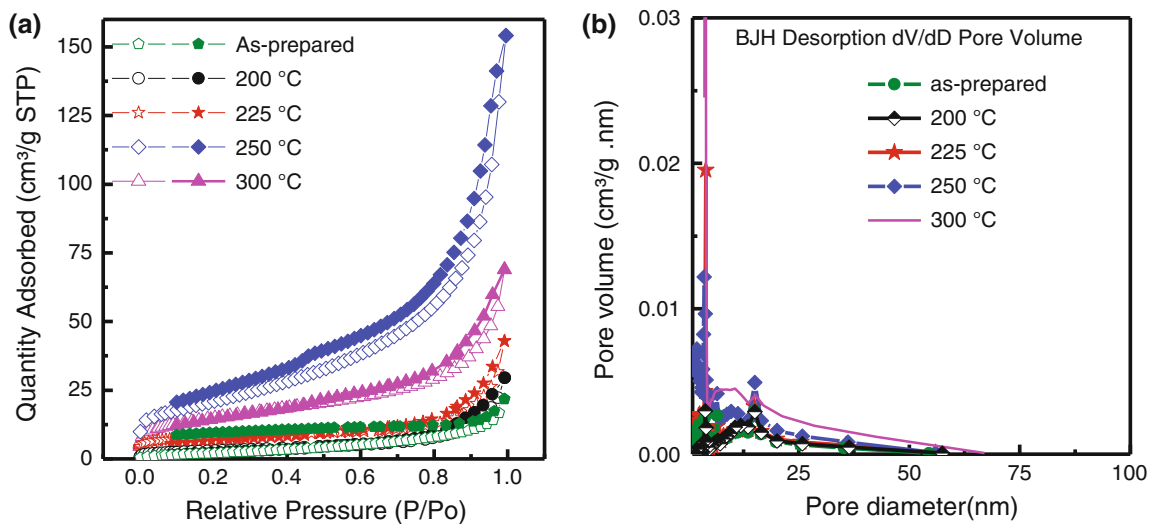
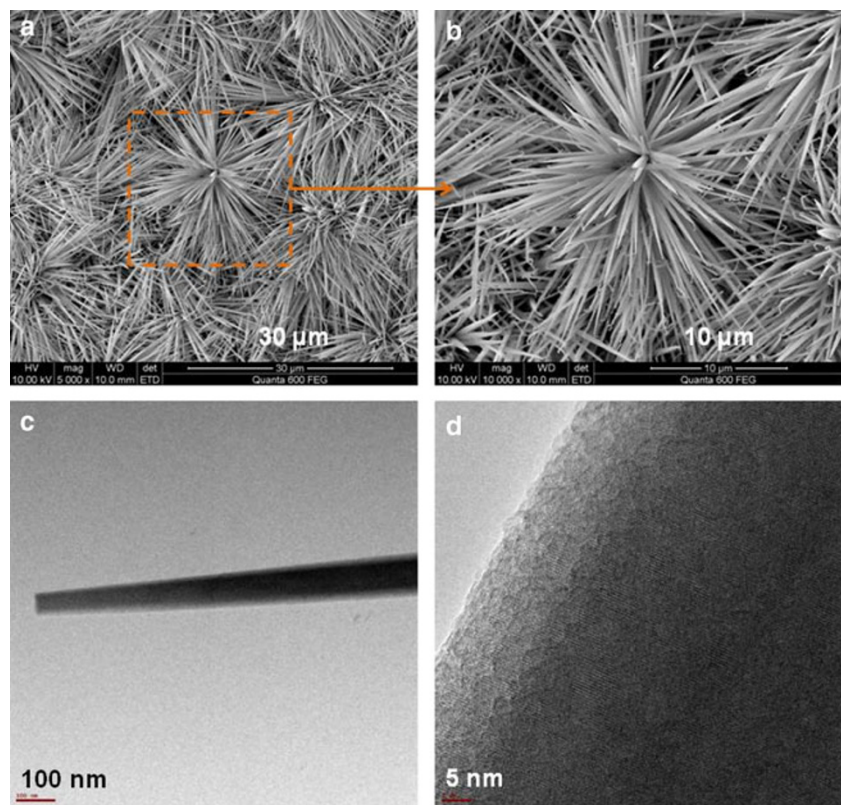


Fig. 2 **a** Nitrogen adsorption and desorption isotherms and **b** pore size distributions of as-prepared and calcined samples

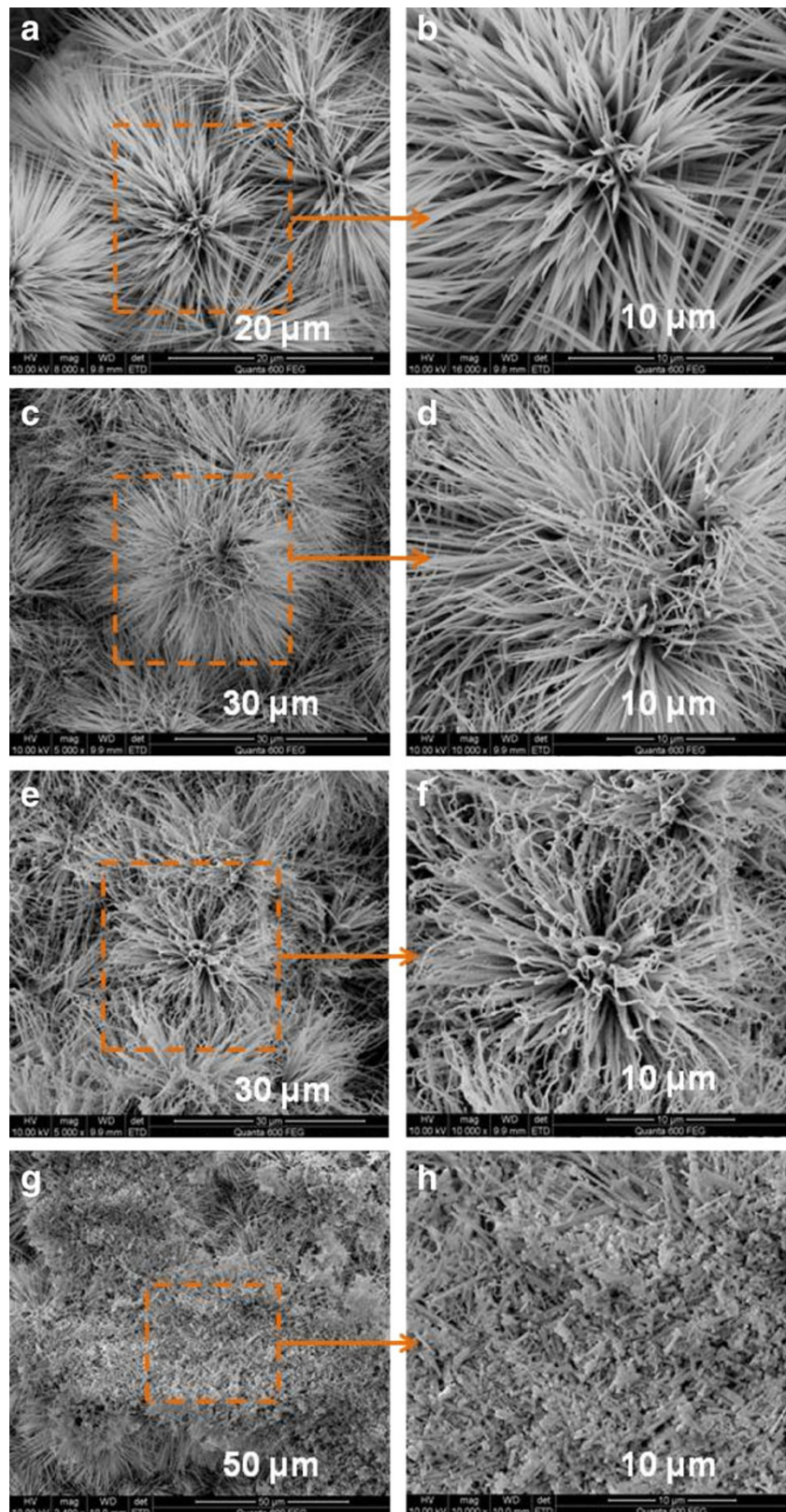
Fig. 3 **a** Low and **b** high magnification SEM images of the as-prepared sample. **c** Low and **d** high magnification TEM images of the as-prepared sample



The effect of calcination temperature on the morphology of Co_3O_4 nanostructures is clearly evident from the low and high magnification SEM images of calcined samples as shown in Fig. 4. Figure 4a and b indicates that calcination at 200 °C resulted in the flattening of rigid sharp cylindrical nanoneedles. With further increase in calcination temperature (at 225 °C), the flowers grow bigger with the center changing into flexible nanowires as shown in Fig. 4c, d. Well-

organized flower-like morphologies of flexible Co_3O_4 nanowires are achieved by calcination of as-prepared samples at 250 °C (Fig. 4e and f). High magnification images indicate that these flower-like structures are composed of cobalt oxide nanowires, with each having a length ranging from 1 to 10 μm. Further increase in calcination temperature (at 300 °C) results in the breaking down of the Co_3O_4 nanowire, destroying the flower-like morphology.

Fig. 4 SEM images of Co_3O_4 nanostructures showing the surface morphology. Low and high magnification SEM images of samples calcined at 200 °C (a and b), 225 °C (c and d), 250 °C (e and f) and 300 °C (g and h)



To investigate the microstructure of Co_3O_4 nanostructures in detail, TEM and HRTEM images are used (Fig. 5). Nanowire calcined at 200 °C (Fig. 5a and b) exhibits the

presence of numerous nanocrystallites of Co_3O_4 having size < 3 nm as compared to the smooth texture of the as-prepared sample. The size of these nanocrystals increases

further with increase in the calcination temperature. The formation of such large crystal structures can probably be attributed to the re-crystallization and aggregation of the particles during calcination, in which the small nanocrystals grow into an interconnected porous structure. From Fig. 4c–h, it is clear that Co_3O_4 nanowires calcined above 225 °C consist of numerous interconnected nanoparticles and presents a rough appearance due to a large number of mesopores. This porous structure can be ascribed to the successive release and loss of H_2O and different gases during the oxidation/decomposition of the intermediate products $\text{Co}(\text{OH})_2$ or cobalt carbonate nitrate hydroxide hydrate. The diameter of the nanowires varies from nearly 160 to 20 nm from the point of contact to the carbon cloth to the tip. For the samples calcined at 250 °C, the mesoporous structure is clearly formed.

The individual nanocrystals have a size in the range of 8–12 nm and the pore sizes are in the range of a few nanometers. Further increase in the calcination temperature to 300 °C leads to the formation of large crystallites having cuboid shape with average size in the range of 16–20 nm, which in turn leads to a reduction in the BET surface area and increase in pore volume.

As the Co_3O_4 nanowires composed of nanocrystallites possess high surface area as well as mesoporosity and are self-organized into flower-like morphologies on the surface of the current collectors, they can be used as efficient electrode materials for supercapacitors. However, the charge storage efficiency of the samples calcined at different temperatures can vary due to the observed differences in orientation and morphology of the 1-D nanostructures. To identify which morphology is favorable for high-rate capacitive energy storage, cyclic voltammetry (CV) and galvanostatic charge–discharge (CD) measurements are conducted in symmetric two-electrode configurations. It has been reported that as compared to three-electrode configuration, measurements using two-electrode configuration is more suited for evaluating the performance of a supercapacitor test cell as it mimics the physical configuration, internal voltages and charge transfer that occurs in a real supercapacitor application and thus provides the best indication of an electrode material's performance [47].

Figure 6a–d, respectively, shows CV loops obtained for symmetric button cell supercapacitors based on Co_3O_4 samples calcined at 200, 225, 250 and 300 °C at different scan rates of 1, 2, 5, 10, 20, 50 and 100 mV/s in a fixed potential range of 0–0.8 V. Test cells of samples calcined above 225 °C retain nearly rectangular CV loops up to a scan rate of 100 mV/s, which are characteristics for supercapacitors with excellent capacitance behavior and low contact resistance. Supercapacitor based on the sample calcined at 200 °C retains symmetric rectangular shape

only up to a scan rate of 20 mV/s. Above 20 mV/s, the CV loops exhibit quasi rectangular shape indicating lower rate performance of the sample as compared to the samples calcined above 225 °C.

Improvement in the performance of samples can be attributed to the formation of mesoporous structure above 225 °C. For samples annealed at 200, 225 and 300 °C, the CV loops at different scan rates show no peaks, which indicate that the electrodes are charged and discharged at a pseudo-constant rate over the complete voltammetric cycle. The CV loops of the supercapacitor based on the sample calcined at 250 °C, shows the presence of a pair of redox peaks indicating the existence of a strong Faradic reaction of Co_3O_4 according to Eq. (3).



A comparison of CV loops of symmetric supercapacitors based on Co_3O_4 samples calcined at different temperatures and carbon cloth substrate at a scan rate of 20 mV/s is shown in Fig. 7a. For the same mass loading, the CV curves show different areas indicating different levels of stored charge. From the CV loops, specific capacitances of 256, 341, 549 and 435 F/g, respectively [using Eqs. (1) and (3)], are obtained for the samples with calcination temperatures 200, 225, 250 and 300 °C. From Fig. 7a, it is also evident that the capacitive contribution from the carbon cloth substrate to the electrodes is negligibly small. Figure 7b shows the comparison of galvanostatic charge discharge curves for the samples at a constant current density of 1 A/g. The constant current charge discharge curves of 1-D Co_3O_4 nanostructures are nearly triangular, with reduced internal resistance at the beginning of the discharge curve. The reduction in internal resistance may be attributable to the direct contact of nanowires and the conducting carbon cloth substrate. The specific capacitance values for the supercapacitors based on samples with calcination temperatures 200, 225, 250 and 300 °C, respectively, are 334, 435, 605 and 509 F/g. Even though the samples calcined at 200 and 250 °C have flower-like morphology, they have less mesopores as compared to the samples calcined at 250 and 300 °C. Hence the electrode–electrolyte accessibility will be less, leading to lower capacitance. The tremendous improvement capacitance for sample calcined at 250 °C can be attributed to the mesoporous nanowire morphology of Co_3O_4 as well as their self-organization into flower-like microarchitecture on the surface of the carbon cloth, capable of holding a large quantity of electrolyte and thereby providing more electrode–electrolyte accessibility. The decrease in the specific capacitance of the sample calcined at 300 °C may be due to the damage in the flower-type morphology, which reduces the quantity of electrolyte trapped in between the

Fig. 5 TEM images of Co_3O_4 nanowires showing a porous structure. Low and high magnification TEM images of samples calcined at 200 °C (a and b), 225 °C (c and d), 250 °C (e and f) and 300 °C (g and h)

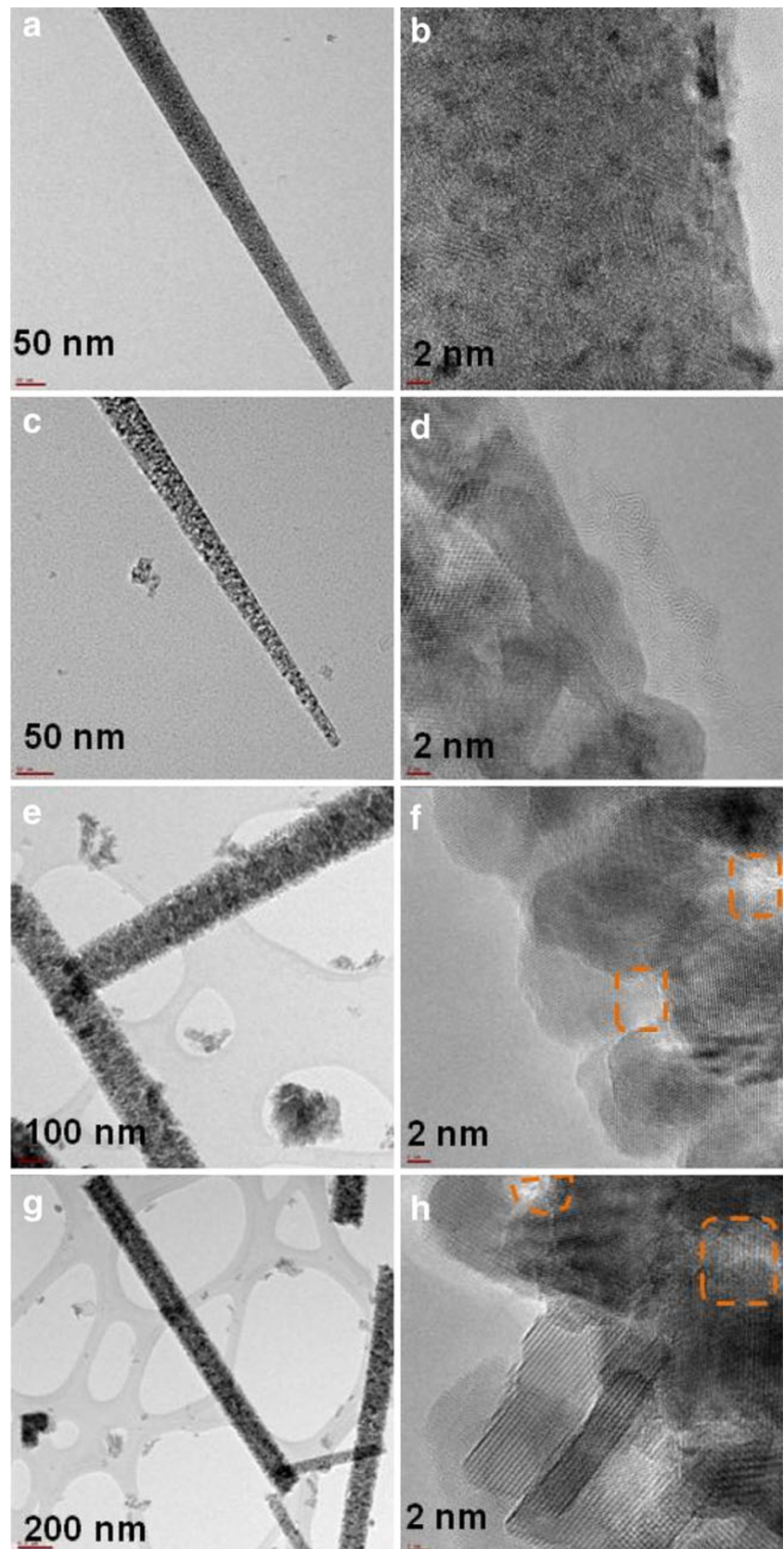
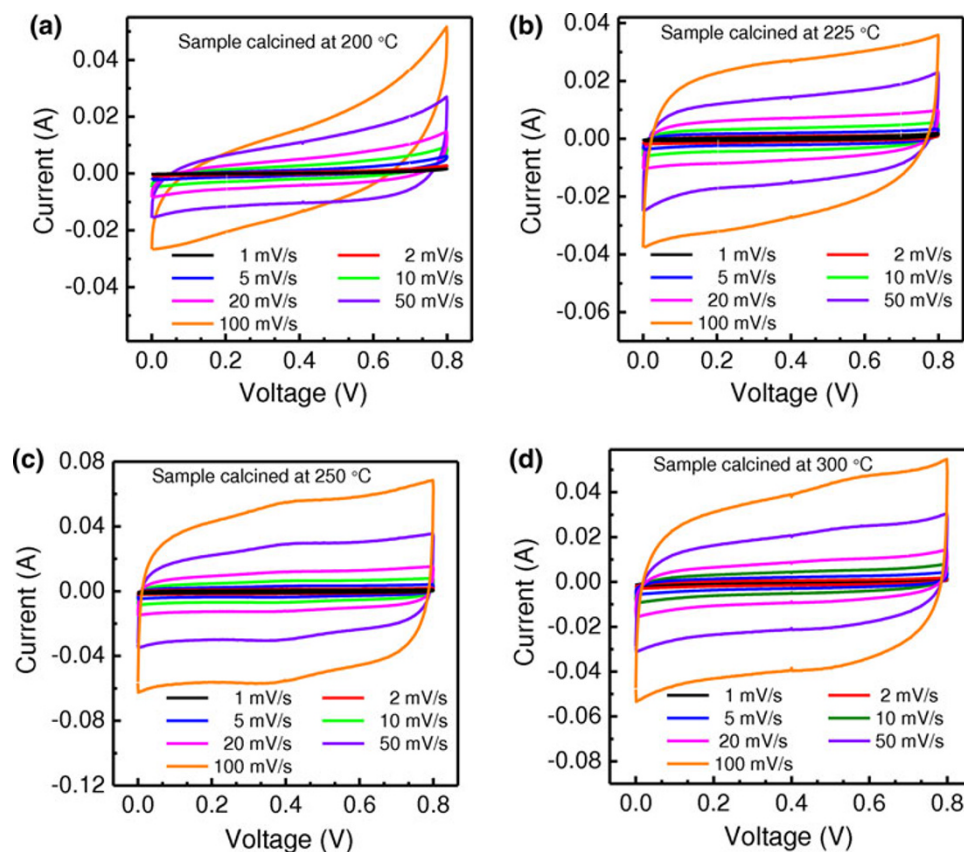


Fig. 6 Cyclic voltammograms of Co_3O_4 samples calcined at **a** 200 °C, **b** 225 °C, **c** 250 °C and **d** 300 °C at different scan rates

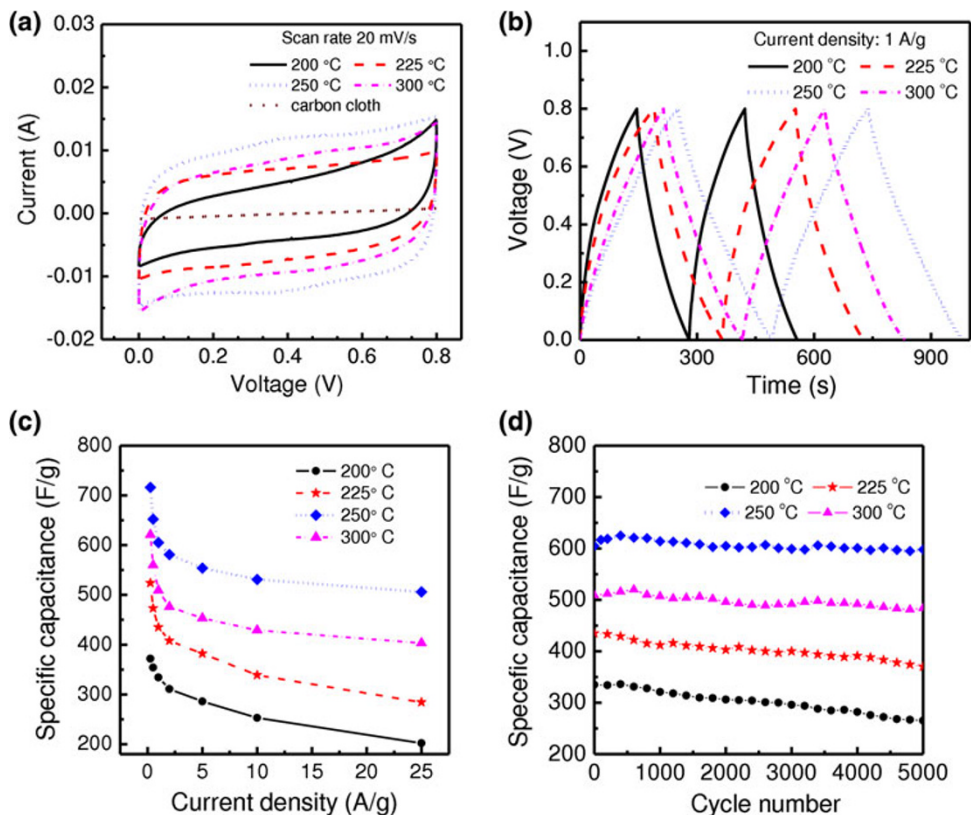


nanowires. But due to the well-formed mesoporous structure, the sample still exhibits higher specific capacitance than the samples calcined at 200 and 225 °C.

High-performance supercapacitor electrodes should have high-rate performance. Variations in specific capacitances of symmetric supercapacitors based on the calcined samples with increase in current density are shown in Fig. 7c. In general, at lower current densities (from 0.25 to 2 A/g), the specific capacitance decreases with the increase in discharge current density; it may be caused by the internal resistance of the electrode. At an extremely low current density of 0.25 A/g, the maximum specific capacitance values for the supercapacitors based on samples with calcination temperatures 200, 225, 250 and 300 °C, respectively, are 372, 524, 716 and 621 F/g. At lower current densities, ions can penetrate into the inner structure of electrode material having access to almost all available pores of the electrode, but at higher current densities an effective utilization of the material is limited only to the outer surface of electrodes. It results in the reduction of specific capacitance values. At current densities above 2 A/g, specific capacitance tends to stabilize. The sample calcined at 250 °C retains more than 83 % of its capacitance (605 F/g at a low current density of 1 A/g) retention even when the current density increases as high as 25 A/g, indicating the relatively good high-rate capability. The

sample calcined at 300 °C is also able to retain 79 % of its capacitance at a high current density of 25 A/g. But samples calcined at 200 and 225 °C are able to retain only 60 and 65 % of their capacitance, due to the incomplete formation of nanocrystallites and mesopores. Cycle life is another important factor for evaluating the performance of a supercapacitor. Cyclic stability curves for symmetric supercapacitors at a constant current density of 1 A/g are illustrated in Fig. 7d. For samples annealed at 250 and 300 °C, the specific capacitance increases gradually at the beginning of cycles and then there is a slight decrease. This phenomenon indicates that there is an initial activation process for Faradaic pseudocapacitance of mesoporous Co_3O_4 . During the first 500 cycles, the specific capacitance of the sample annealed at 250 °C increases from 605 to 625 F/g and that of Co_3O_4 nanowires with flower-like morphology increases from 509 to 520 F/g. For the samples annealed at 250 and 300 °C, the specific capacitance slowly decreases with increase in cycle numbers. At the end of 5,000 cycles, supercapacitors based on samples with calcination temperatures 200, 225, 250 and 300 °C retain, respectively, 80, 85, 97 and 93 % of their maximum capacitance. Direct growth of 1-D Co_3O_4 nanostructures on carbon substrates and the self-organization of nanostructures into flower-like microarchitectures also have dramatic impact on supercapacitor performance, as each

Fig. 7 **a** Comparison of cyclic voltammograms of Co_3O_4 samples and carbon cloth substrate at a scan rate of 20 mV/s. **b** Comparison of charge–discharge curves of calcined Co_3O_4 samples at a constant current density of 1 A/g. **c** Specific capacitances of calcined Co_3O_4 samples at different current densities. **d** Cycling performance of calcined Co_3O_4 samples at a constant current density of 1 A/g (5,000 charge–discharge cycles)

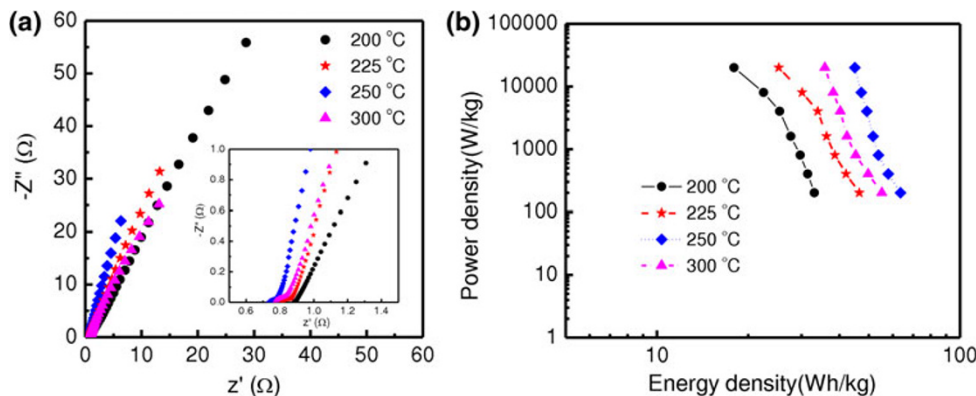


nanostructure will be electronically attached to the current collector which in turn will reduce the internal resistance of the electrode facilitating the rapid transport of the electrolyte ions and increasing the electrochemical utilization and pseudocapacitive performance of Co_3O_4 .

Electrochemical impedance spectroscopy (EIS) can be applied to investigate electrical conductivity and ion transfer of the supercapacitor test cells. Figure 8a shows the experimental Nyquist impedance spectra for symmetric supercapacitor test cells of Co_3O_4 samples prepared at different calcination temperatures. The impedance spectra can be divided into two regions by the so-called knee frequency, with a semicircle arc in the high-frequency

region and a straight line in the low-frequency region. The real axis intercept at high frequency corresponds to the uncompensated resistance of the bulk electrolyte solution (R_s) and it is also known as equivalent series resistance (ESR). The diameter of semicircle in the high-frequency range gives the value of charge transfer resistance (R_{ct}). R_{ct} is a surface property of the porous electrode which is related to the electroactive surface area. It is a combination of electrolyte accessible area and electrical conductivity of the electrode material. The larger the electroactive surface area, the lower is the charge transfer resistance. In the present study all the samples exhibit very low value for R_{ct} , indicating high conductivity of the electrodes with

Fig. 8 **a** Nyquist plots for supercapacitors based on calcined Co_3O_4 samples. **b** Ragone plot (power density vs. energy density) of calcined Co_3O_4 samples based on symmetric supercapacitors. The energy densities and power densities were derived from the charge–discharge curves at different current densities



excellent electrolyte accessibility. The line at the low-frequency region making an angle 45° with the real axis is the Warburg line, which is a result of the frequency dependence of ion diffusion in the electrolyte to the electrode interface. Experimental results show that the magnitude of ESR obtained from the x -intercept of the impedance spectra for supercapacitors based on Co_3O_4 samples prepared at calcination temperatures 200, 225, 250 and 300°C are 0.88, 0.81, 0.73 and $0.76\ \Omega$, respectively. These lower values indicate consistent interfacial contact between the cobalt oxide nanowires and the carbon substrates. ESR data are an important factor in determining the maximum possible power density of a supercapacitor. The maximum power density (P_{max}) of the supercapacitor devices are calculated from the low-frequency data of the impedance spectra, according to the Eq. (4).

$$P_{\text{max}} = \frac{V_i^2}{4MR} \quad (4)$$

where V_i is the initial voltage (here it is 1 V), R is ($R_s + R_{\text{ct}}$) and M is the total mass of two electrodes with a cell voltage of 0.8 V. Maximum power densities of 31.9, 34.6, 38.5 and $35.5\ \text{kW/kg}$ are obtained, respectively, for supercapacitors based on Co_3O_4 samples prepared at calcination temperatures of 200, 225, 250 and 300°C .

Figure 8b shows the Ragone plot (power density vs. energy density) of the symmetric supercapacitors based on Co_3O_4 calcined at different temperatures. The energy (E) and power densities (P) for the supercapacitors were calculated from charge–discharge curves at different current densities using Eq. (5) and (6), respectively.

$$E = \frac{1}{2} C_{\text{sp}} \Delta V^2 \quad (5)$$

where ' ΔV ' is the potential window of the discharge process.

$$P = E/\Delta t \quad (6)$$

At a constant power density of $20\ \text{kW/kg}$, the energy densities obtained for supercapacitors based on samples with calcination temperatures 200, 225, 250 and 300°C are 17, 25, 44 and $35\ \text{Wh/kg}$, respectively. At a low power density of $0.2\ \text{kW/kg}$, the energy densities reach as high as 33, 47, 63 and $55\ \text{Wh/kg}$, respectively, for the samples calcined at 200, 225, 250 and 300°C . From the analysis of Ragone plot, it is evident that mesoporous Co_3O_4 nanowires prepared by the calcination of the as-prepared sample at 250°C works as a very promising electrode material for high-performance supercapacitors. This sample maintains a high power density without much reduction in energy density.

The present study clearly demonstrates that calcination temperature plays a significant role in tuning the

morphology, porosity and capacitive performance of 1-D Co_3O_4 nanostructures. By changing calcination temperature from 200°C (flattened nanoneedles) to 250°C (mesoporous nanowires), we could nearly double the maximum capacitance of the Co_3O_4 . The flower-like self-organization of mesoporous Co_3O_4 nanowires obtained by the calcination of as-prepared sample at 250°C exhibits superior supercapacitor performance as compared to the other three samples. This can be attributed to the mesoporous nanowire morphology of Co_3O_4 retaining the flower-like microarchitecture, which accelerates the Faradaic charge transfer reactions, by providing easy diffusion of KOH electrolyte between different nanowires, accessing almost all the nanowires over the entire sample. In a recent study we reported a maximum pseudocapacitance of $620\ \text{F/g}$ at a current density of $0.25\ \text{A/g}$ for Co_3O_4 nanowires with flower-like morphology directly grown over carbon paper. Improvement in capacitive performance of a similar sample grown over carbon cloth substrate in the present study can be attributed to the improved wettability of the carbon cloth. It is interesting to note that even in two-electrode configuration with a high mass loading of $2\ \text{mg}$ per electrode, the sample calcined at 250°C yields higher pseudocapacitance and rate performance behavior than most of the previously reported Co_3O_4 electrodes.

Conclusions

In summary, we have demonstrated that the calcination temperature plays a crucial role in tuning the nanostructure and pseudocapacitive performance of mesoporous Co_3O_4 nanowires grown directly over carbon cloth substrate. The Co_3O_4 nanostructure sample calcined at 250°C exhibited the best capacitive performance with high specific capacitance values ($716\ \text{F/g}$ at $0.25\ \text{A/g}$ and $605\ \text{F/g}$ at $1\ \text{A/g}$), high-rate performance (83 %) and excellent cycling stability (97 % after 5,000 charge discharge cycles) when used in symmetric two-electrode configuration. This improvement in the performance was attributed to the mesoporous nature of the Co_3O_4 nanowires retaining the flower-like morphology and providing maximum access of aqueous electrolyte to the electrodes.

Acknowledgments The authors thank the 'Advanced nanofabrication, Imaging and Characterization Laboratory' and 'Analytic Core Laboratory', KAUST. R. B. R. acknowledges the financial support from SABIC Postdoctoral Fellowship. W. C. acknowledges support from KAUST Graduate Fellowship. H. N. A. acknowledges the generous support from KAUST Baseline Fund.

Open Access This article is distributed under the terms of the Creative Commons Attribution License which permits any use, distribution, and reproduction in any medium, provided the original author(s) and the source are credited.

References

- Simon, P., Gogotsi, Y.: Materials for electrochemical capacitors. *Nat Mater* **7**(11), 845–854 (2008). doi:10.1038/nmat2297
- Conway, B.E.: *Electrochemical supercapacitors: scientific fundamentals and technological applications*. Kluwer Academic/Plenum, New York (1999)
- Jayalakshmi, M., Balasubramanian, K.: Simple capacitors to supercapacitors—an overview. *Int J Electrochem Sci* **3**(11), 1196–1217 (2008)
- Xu, J.J., Wang, K., Zu, S.Z., Han, B.H., Wei, Z.X.: Hierarchical nanocomposites of polyaniline nanowire arrays on graphene oxide sheets with synergistic effect for energy storage. *ACS Nano* **4**(9), 5019–5026 (2010). doi:10.1021/nn1006539
- Benson, J., Boukhalfa, S., Magasinski, A., Kvit, A., Yushin, G.: Chemical vapor deposition of aluminum nanowires on metal substrates for electrical energy storage applications. *ACS Nano* **6**(1), 118–125 (2012). doi:10.1021/nn202979y
- Jacob, G.M., Yang, Q.M., Zhitomirsky, I.: Composite electrodes for electrochemical supercapacitors. *J Appl Electrochem* **39**(12), 2579–2585 (2009). doi:10.1007/s10800-009-9953-8
- Naoui, K.: ‘Nanohybrid capacitor’: the next generation electrochemical capacitors. *Fuel Cells* **10**(5), 825–833 (2010). doi:10.1002/fuce.201000041
- Pumera, M.: Graphene-based nanomaterials for energy storage. *Energy Environ Sci* **4**(3), 668–674 (2011)
- Chen, W., Rakhi, R.B., Hu, L.B., Xie, X., Cui, Y., Alshareef, H.N.: High-performance nanostructured supercapacitors on a sponge. *Nano Lett* **11**(12), 5165–5172 (2011). doi:10.1021/nl2023433
- Rakhi, R.B., Chen, W., Cha, D., Alshareef, H.N.: Nanostructured ternary electrodes for energy-storage applications. *Adv Energy Mater* **2**(3), 381–389 (2012). doi:10.1002/aenm.201100609
- Wang, G.P., Zhang, L., Zhang, J.J.: A review of electrode materials for electrochemical supercapacitors. *Chem Soc Rev* **41**(2), 797–828 (2012). doi:10.1039/c1cs15060j
- Zhang, H., Cao, G.P., Yang, Y.S.: Carbon nanotube arrays and their composites for electrochemical capacitors and lithium-ion batteries. *Energy Environ Sci* **2**(9), 932–943 (2009). doi:10.1039/b906812k
- Pandolfo, A.G., Hollenkamp, A.F.: Carbon properties and their role in supercapacitors. *J Power Sour* **157**(1), 11–27 (2006). doi:10.1016/j.jpowsour.2006.02.065
- Liu, C.G., Liu, M., Wang, M.Z., Cheng, H.M.: Research and development of carbon materials for electrochemical capacitors—II—The carbon electrode. *New Carbon Mater* **17**(2), 64–72 (2002)
- Lota, G., Fic, K., Frackowiak, E.: Carbon nanotubes and their composites in electrochemical applications. *Energy Environ Sci* **4**(5), 1592–1605 (2011)
- Biener, J., Stadermann, M., Suss, M., Worsley, M.A., Biener, M.M., Rose, K.A., Baumann, T.F.: Advanced carbon aerogels for energy applications. *Energy Environ Sci* **4**(3), 656–667 (2011)
- Li, X., Rong, J.P., Wei, B.Q.: Electrochemical behavior of single-walled carbon nanotube supercapacitors under compressive stress. *ACS Nano* **4**(10), 6039–6049 (2010). doi:10.1021/nn101595y
- Izadi-Najafabadi, A., Yamada, T., Futaba, D.N., Yudasaka, M., Takagi, H., Hatori, H., Iijima, S., Hata, K.: High-power supercapacitor electrodes from single-walled carbon nanohorn/nanotube composite. *ACS Nano* **5**(2), 811–819 (2011). doi:10.1021/nn1017457
- Zheng, J.P., Cygan, P.J., Jow, T.R.: Hydrous ruthenium oxide as an electrode material for electrochemical supercapacitors. *J Electrochem Soc* **142**(8), 2699–2703 (1995)
- Xu, C.J., Kang, F.Y., Li, B.H., Du, H.D.: Recent progress on manganese dioxide based supercapacitors. *J Mater Res* **25**(8), 1421–1432 (2010). doi:10.1557/jmr.2010.0211
- Guan, C., Liu, J.P., Cheng, C.W., Li, H.X., Li, X.L., Zhou, W.W., Zhang, H., Fan, H.J.: Hybrid structure of cobalt monoxide nanowire @ nickel hydroxidenitrate nanoflake aligned on nickel foam for high-rate supercapacitor. *Energy Environ Sci* **4**(11), 4496–4499 (2011). doi:10.1039/c1ee01685g
- Mai, L.Q., Yang, F., Zhao, Y.L., Xu, X., Xu, L., Luo, Y.Z.: Hierarchical MnMoO(4)/CoMoO(4) heterostructured nanowires with enhanced supercapacitor performance. *Nature Commun* **2**, 381 (2011). doi:10.1038/ncomms1387
- Dong, S., Chen, X., Gu, L., Zhou, X., Li, L., Liu, Z., Han, P., Xu, H., Yao, J., Wang, H., Zhang, X., Shang, C., Cui, G., Chen, L.: One dimensional MnO₂/titanium nitride nanotube coaxial arrays for high performance electrochemical capacitive energy storage. *Energy Environ Sci* **4**(9), 3502–3508 (2011)
- Yan, J.A., Khoo, E., Sumboja, A., Lee, P.S.: Facile coating of manganese oxide on tin oxide nanowires with high-performance capacitive behavior. *ACS Nano* **4**(7), 4247–4255 (2010). doi:10.1021/nn100592d
- Rakhi, R.B., Chen, W., Cha, D.Y., Alshareef, H.N.: Substrate dependent self-organization of mesoporous cobalt oxide nanowires with remarkable pseudocapacitance. *Nano Lett* **12**(5), 2559–2567 (2012). doi:10.1021/nl300779a
- Yang, L., Cheng, S., Ding, Y., Zhu, X.B., Wang, Z.L., Liu, M.L.: Hierarchical network architectures of carbon fiber paper supported cobalt oxide nanonet for high-capacity pseudocapacitors. *Nano Lett* **12**(1), 321–325 (2012). doi:10.1021/nl203600x
- Qing, X.X., Liu, S.Q., Huang, K.L., Lv, K.Z., Yang, Y.P., Lu, Z.G., Fang, D., Liang, X.X.: Facile synthesis of Co(3)O(4) nanoflowers grown on Ni foam with superior electrochemical performance. *Electrochim Acta* **56**(14), 4985–4991 (2011). doi:10.1016/j.electacta.2011.03.118
- Xia, X.H., Tu, J.P., Zhang, Y.Q., Wang, X.L., Gu, C.D., Zhao, X.B., Fan, H.J.: High-quality metal oxide core/shell nanowire arrays on conductive substrates for electrochemical energy storage. *ACS Nano* **6**(6), 5531–5538 (2012). doi:10.1021/nm301454q
- Sassin, M.B., Chervin, C.N., Rolison, D.R., Long, J.W.: Redox deposition of nanoscale metal oxides on carbon for next-generation electrochemical capacitors. *Acc Chem Res* **46**(5), 1062–1074 (2013). doi:10.1021/ar2002717
- Yu, G.H., Xie, X., Pan, L.J., Bao, Z.N., Cui, Y.: Hybrid nanostructured materials for high-performance electrochemical capacitors. *Nano Energy* **2**(2), 213–234 (2013). doi:10.1016/j.nanoen.2012.10.006
- Xia, X.H., Tu, J.P., Mai, Y.J., Wang, X.L., Gu, C.D., Zhao, X.B.: Self-supported hydrothermal synthesized hollow Co(3)O(4) nanowire arrays with high supercapacitor capacitance. *J Mater Chem* **21**(25), 9319–9325 (2011). doi:10.1039/c1jm10946d
- Meher, S.K., Rao, G.R.: Ultralayered Co(3)O(4) for high-performance supercapacitor applications. *J Phys Chem C* **115**(31), 15646–15654 (2011). doi:10.1021/jp201200e
- Zhang, F.Z.C.Y.X.L.L.Z.Q.C.X.: Facile growth of mesoporous Co₃O₄ nanowire arrays on Ni foam for high performance electrochemical capacitors. *J Power Sources* **203**, 250–256 (2012)
- Zhang, L.C.J.L.X.G.: Preparation and properties of Co₃O₄ nanorods as supercapacitor material. *J Appl Electrochem* **39**, 1871–1876 (2009)
- Wang, H.Z.L., Tan, X., Hol, C.M.B., Zahiri, B., Olsen, B.C., Mitlin, D.: Supercapacitive properties of hydrothermally synthesized Co₃O₄ nanostructures. *J Phys Chem C* **115**, 17599–17605 (2011)
- Kandalkar, S.G., Lee, H.M., Chae, H., Kim, C.K.: Structural, morphological, and electrical characteristics of the electrodeposited cobalt oxide electrode for supercapacitor applications.

- Mater Res Bull **46**(1), 48–51 (2011). doi:[10.1016/j.materresbull.2010.09.041](https://doi.org/10.1016/j.materresbull.2010.09.041)
37. Wu, J.B., Lin, Y., Xia, X.H., Xu, J.Y., Shi, Q.Y.: Pseudocapacitive properties of electrodeposited porous nanowall Co(3)O(4) film. *Electrochim Acta* **56**(20), 7163–7170 (2011). doi:[10.1016/j.electacta.2011.05.067](https://doi.org/10.1016/j.electacta.2011.05.067)
38. Tummala, R., Guduru, R.K., Mohanty, P.S.: Nanostructured Co₃O₄ electrodes for supercapacitor applications from plasma spray technique. *J Power Sources* **209**, 44–51 (2012). doi:[10.1016/j.jpowsour.2012.02.071](https://doi.org/10.1016/j.jpowsour.2012.02.071)
39. Asano, Y., Komatsu, T., Murashiro, K., Hoshino, K.: Capacitance studies of cobalt compound nanowires prepared via electrodeposition. *J Power Sources* **196**(11), 5215–5222 (2011). doi:[10.1016/j.jpowsour.2011.01.101](https://doi.org/10.1016/j.jpowsour.2011.01.101)
40. Xu, J.A., Gao, L., Cao, J.Y., Wang, W.C., Chen, Z.D.: Preparation and electrochemical capacitance of cobalt oxide (Co(3)O(4)) nanotubes as supercapacitor material. *Electrochim Acta* **56**(2), 732–736 (2010). doi:[10.1016/j.electacta.2010.09.092](https://doi.org/10.1016/j.electacta.2010.09.092)
41. Xia, X.H., Tu, J.P., Zhang, Y.Q., Mai, Y.J., Wang, X.L., Gu, C.D., Zhao, X.B.: Freestanding Co₃O₄ nanowire array for high performance supercapacitors. *Rsc Advances* **2**(5), 1835–1841 (2012). doi:[10.1039/c1ra00771h](https://doi.org/10.1039/c1ra00771h)
42. Lu, X., Zheng, D., Zhai, T., Liu, Z., Huang, Y., Xie, S., Tong, Y.: Facile synthesis of large-area manganese oxide nanorod arrays as a high-performance electrochemical supercapacitor. *Energy Environ Sci* **4**(8), 2915–2921 (2011)
43. Gao, Y.Y., Chen, S.L., Cao, D.X., Wang, G.L., Yin, J.L.: Electrochemical capacitance of Co(3)O(4) nanowire arrays supported on nickel foam. *J Power Sources* **195**(6), 1757–1760 (2010). doi:[10.1016/j.jpowsour.2009.09.048](https://doi.org/10.1016/j.jpowsour.2009.09.048)
44. Xing, W., Qiao, S.Z., Wu, X.Z., Gao, X.L., Zhou, J., Zhuo, S.P., Hartono, S.B., Hulicova-Jurcakova, D.: Exaggerated capacitance using electrochemically active nickel foam as current collector in electrochemical measurement. *J Power Sources* **196**(8), 4123–4127 (2011). doi:[10.1016/j.jpowsour.2010.12.003](https://doi.org/10.1016/j.jpowsour.2010.12.003)
45. Jost, K., Perez, C.R., McDonough, J.K., Presser, V., Heon, M., Dion, G., Gogotsi, Y.: Carbon coated textiles for flexible energy storage. *Energy Environ Sci* **4**(12), 5060–5067 (2011)
46. Xiong, S., Yuan, C., Zhang, X., Xi, B., Qian, Y.: Controllable synthesis of mesoporous Co₃O₄ nanostructures with tunable morphology for application in supercapacitors. *Chem Eur J* **15**, 5320–5326 (2009)
47. Stoller, M.D., Ruoff, R.S.: Best practice methods for determining an electrode material's performance for ultracapacitors. *Energy Environ Sci* **3**(9), 1294–1301 (2010). doi:[10.1039/c0ee00074d](https://doi.org/10.1039/c0ee00074d)